ENGINEER - Vol. LVII, No. 03, pp. [95-106], 2024

DOI: https://doi.org/10.4038/engineer.v57i3.7659

# Enhancing the Seismic Performances of Concrete Filled Steel Box Columns by Improving Confinement Effect: A Numerical Approach

**A.M.Y.D. Alahakoon, V.P. Malalage, A.C.D. Pigera and J.A.S.C. Jayasinghe**

**Abstract:** Highway piers are essential in elevated roadways, and they are widely used in industrialized nations. Therefore, designing piers that can withstand severe seismic loadings is critical, especially in regions where earthquakes are common. Because of their remarkable seismic resilience, concrete-filled steel tubular (CFST) columns have become more popular. Numerous investigations have been carried out to enhance the seismic performance of CFST columns. The goal of this study is to alter the stiffener arrangements of concrete-filled steel box columns in order to increase their strength, ductility, energy absorption capacity and hence enhance their overall performance by enhancing the confinement effect. A comprehensive finite element model of CFST column with stiffeners was developed and validated using past experimental data. By adopting the same modelling procedure, ten models of CFST columns with modified cross sections by changing the stiffener length, stiffener arrangement and flange to web ratio of stiffeners were numerically tested under lateral cyclic loads with constant axial loads to understand the effective cross section for the confinement effect. Results revealed that the T arrangement of stiffeners shows an increment in confinement effect which results in enhancement of lateral performance of the column. Further enhancement of the confinement was obtained by changing the flange to web ratio ($L_f/L_w$) of the stiffeners. Finally, the obtained force-displacement curves were compared to investigate the effect of confinement and it was revealed that the cross-section having the ratio of $L_f$ / $L_w$ = 2.0 performs better than the other cross-sectional arrangements in strength and for the energy absorption capacity, while $L_f$ / $L_w$ = 1.0 is the best arrangement for the ductility.

**Keywords:** Concrete-filled steel tube, Confinement effect, Cyclic loading, Finite element model, Seismic performance

## 1. Introduction

Steel piers are becoming much more popular in the civil engineering industry due to their performance compared to their concrete counterparts [1]. They are mainly used in constructing bridge piers, transmission towers, and overpasses. Ability of these structures to withstand severe earthquakes depends on their strength, ductility and energy absorption capacity.

In the history of bridge construction, steel bridge piers played a pivotal role before the widespread adoption of concrete-filled steel tubular (CFST) columns. The use of steel bridge piers was prevalent in early to mid 20th century, representing a traditional approach to providing structural support to bridges. As mentioned in Zarringol et al., *(2020)*, typical damage to the steel bridge piers are classified into local buckling, brittle crack failure and low cycle fatigue failure [2]. These structures undergo severe seismic loadings in earthquake prone areas. Hence, to mitigate such failures, higher strength, ductility and energy absorption capacity of the structural system is essential, which would result in better seismic performances of steel bridge piers. Several techniques are adopted to enhance the perfomance of steel bridge piers, such as providing different stiffener arrangements,

*Eng.* ***A.M.Y.D. Alahakoon**, AMIE(SL), B.Sc. Eng. (Hons) (Peradeniya), Department of Civil Engineering, Faculty of Engineering, University of Peradeniya, Sri Lanka.*
*Email:e17007@eng.pdn.ac.lk*
*https://orcid.org/0009-0007-8303-9099*
*Eng.* ***V.P. Malalage,** AMIE(SL), B.Sc. Eng. (Hons) (Peradeniya), Department of Civil Engineering, Faculty of Engineering, University of Peradeniya, Sri Lanka.*
*Email: e17204@eng.pdn.ac.lk*
*https://orcid.org/0009-0006-8573-467x*
*Eng.* ***A.C.D. Pigera,** AMIE(SL), B.Sc. Eng. (Hons) (Peradeniya), Department of Civil Engineering, Faculty of Engineering, University of Peradeniya, Sri Lanka.*
*Email: e16283@eng.pdn.ac.lk*
*https://orcid.org/0009-0006-4290-7331*
*Eng.* ***(Dr.) J.A.S.C. Jayasinghe**, AMIE(SL), B.Sc. Eng. (Hons) (Peradeniya), M.Eng. (AIT), PhD. (Tokyo), Senior Lecturer in Department of Civil Engineering, University of Peradeniya, Sri Lanka.*
*Email:supunj@pdn.ac.lk*
*https://orcid.org/0000-0003-1054-9358*

double column arrangements, concrete filling and providing energy dissipation methods [3-11], which are shown in Figure 1.

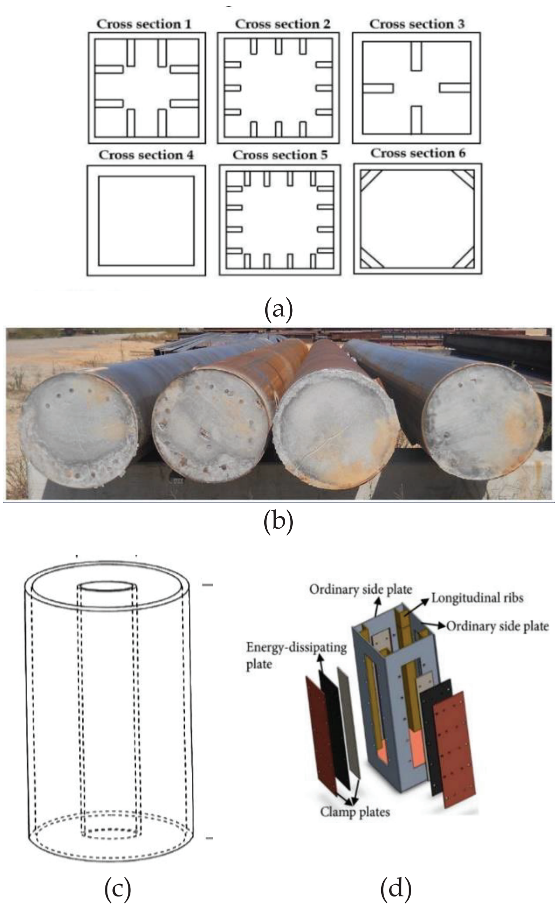


**Figure 1 - Improvement Methods for Steel Piers: (a) different Stiffener Arrangements (b) Concrete Filling (c) Double Column Arrangement and (d) Energy Dissipation Methods**

However, the incorporation of concrete filling method represents a significant advancement in enhancing the performance of steel columns in bridge construction. Steel-encased CFST box members have been recently used as piers in bridges owing to their high stiffness and strength compared to the conventional steel columns [12]. These structures consist of a concrete core encased with steel plates. This combination of steel and concrete creates a composite column that takes advantage of high strength, better ductility and enhancement of energy absorption capacity than the conventional steel bridge piers. The combination of the CFST columns with stiffeners represent a significant stride in strengthening their seismic performances than the CFSTs without stiffener as shown in Figure 2 [13]. Stiffeners which are strategically added to the interior of the steel plate, serve to enhance their lateral stability and resistance to seismic forces. These stiffeners effectively mitigate the risk of buckling and improve the overall capacity of the column to withstand dynamic loads during earthquakes.

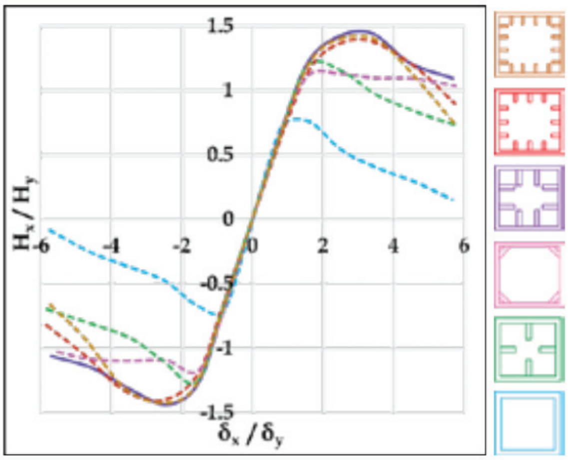


**Figure 2 - Comparison of the Lateral Performance of Piers with and without Stiffeners [14]**

However, the seismic behaviour of CFST with stiffener members has not been thoroughly investigated, which hinders the usage of such members in earthquake-prone zones [12]. Several past studies focused on different ways to improve the seismic performance of CFST columns such as optimizing material properties of the steel tube and the concrete fill, improving the interaction between the steel tube and the concrete filling, and enhancing the behaviour of CFST column joints [15].

Achieving a further enhancement in seismic performance involves the innovative approach of confining the concrete within the CFST with stiffener columns. Increment of the strength and ductility in confined concrete compared to unconfined concrete is shown in Figure 3 [16]. Both experimental and numerical studies conducted to investigate the effect of confinement on the strength, ductility, and energy absorption capacity of CFST columns are rare and the current design guidelines are mainly relying on empirical formulas which only consider effect of the column axial load and slenderness ratio [17]. Therefore, the aim of this paper is to enhance the seismic performances of partially concrete-filled steel box columns by improving the confinement effect with different stiffener arrangements.

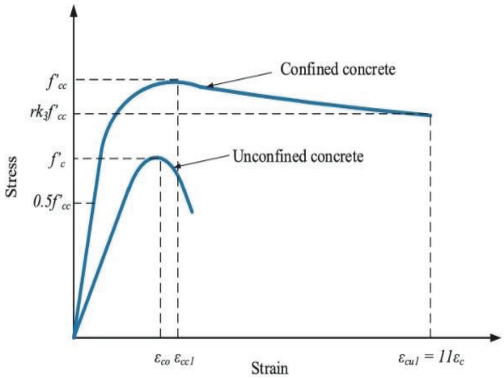


**Figure 3 - Stress Strain Curve of Confined and Unconfined Concrete [16]**

To perform this study, stiffener lengths, stiffener spacings and stiffener arrangements were changed to enhance the confinement, and ultimately the strength, ductility and energy absorption capacity. Finally, the stiffened steel columns with concrete cores having different cross-sectional arrangements were analysed numerically. Analysis was carried out using "*ABAQUS*" finite element software, in which the effect of both material and geometric nonlinearities was considered. The study will contribute to the effective seismic strengthening technique for the CFST columns.

The lateral performances were compared and evaluated using the hysteresis envelop curves where the researchers evaluated the strength and ductility performances due to the strengthening techniques. Performance indices which are used to compare the lateral performance of structures such as lateral load and the lateral displacement at the yield point ($H_y$ , $\delta_y$) and the maximum lateral load and the corresponding lateral displacement ($H_m$ , $\delta_m$) are shown in Figure 4 [18].

In this study, the developed finite element model of CFST column with stiffeners was validated using past experimental data from the literature [1]. Then, a parametric study was conducted by varying the stiffener length, stiffener arrangement and stiffener spacing to identify the most effective cross section towards the enhancement of seismic performance. Finally, the results obtained were compared, discussed and conclusions were made to select the effective cross sections for the enhancement of strength, ductility, and energy absorption.

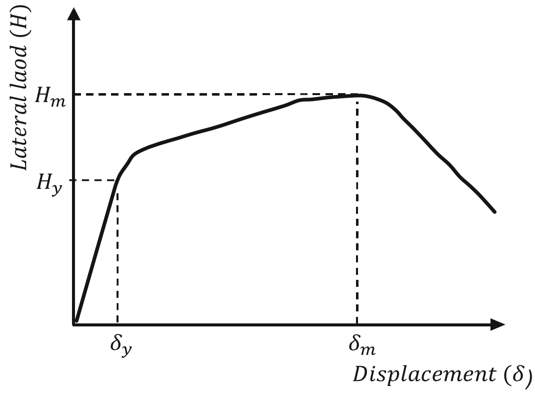


**Figure 4 - Hysteresis Envelop Curve under Lateral Cyclic Loading [18]**

## 2. Finite Element Analysis of CFST Column

In the earlier stage of research, experimental analyses were predominantly relied upon to understand the seismic behaviour of structures. However, as a result of advancement of sophisticated numerical modelling techniques and the availability of powerful computational tools, research is now increasingly turning towards numerical simulations for more comprehensive and efficient seismic analysis of CFST columns. Several studies have been carried out on the improvement methods of steel hollow columns, structural behaviour of the CFST, loading arrangements, confinement effect of the CFST and numerical modelling of steel and concrete materials. Among the previous studies, several analytical methods to perform the nonlinear simulations can be identified such as empirical model, plastic hinge model and elasto-plastic finite element model [19-21]. In the comparisons with experimental data, it shows that the finite element (FE) model predicts the behaviour of these structures more accurately with the availability of wide range of nonlinear capabilities such as material nonlinearities, geometric nonlinearities, and surface contacts. Also, several failure modes can be identified using the FE model, and it can visually represent various physical parameters such as stress, deflection and temperature. Even though finite element modelling of CFST piers has such advantages, constraints such as assuming the stress - strain curve in material model to a bilinear curve and neglecting the localized geometric imperfections in fabrication of structures are some of the shortcomings observed in the current study.

### 2.1 Material Models

Material models which are included in ABAQUS FE software for both concrete and steel were used with the parameters calibrated for the specific materials used in the selected experiment. In concrete, two main regions can be identified in material behaviour, which are named as elastic region and failure region with plastic deformations. Simple linear elasticity theory was used with Young's modulus and Poison's ratio to model the elastic region of the concrete material. There are mainly four models to capture the irreversible deformations and failure envelop of the plastic state (namely smeared crack model), brittle crack model, concrete damage plasticity (CDP) model and Mohr-Coulomb failure criterion model. It is difficult to predict localised failures using smeared crack model, and in brittle crack model, it only considers the elastic behaviour. However, the CDP model describes the best inelastic behaviour of concrete with overcoming the drawbacks of other models.

#### 2.1.1 Concrete Damage Plasticity Model

The concrete damage plasticity (CDP) model was used to model the concrete material. A methodology proposed by Alfrah et al. [24] to predict the concrete's uni-axial stress-strain curve was used in this study. $\sigma_{cu}$ and $\sigma_{t0}$ represent the compressive strength and the tensile strength, respectively, in Figures 5 and 6, whereas $\varepsilon_{cm}$ and $\varepsilon_{tm}$ represent the corresponding strains. $\varepsilon_C^{in}$ and $\varepsilon_{0C}^{el}$ in Figure 5 denote the crushing and elastic undamaged strain components, respectively, while $\varepsilon_C^{pl}$ and $\varepsilon_C^{el}$ show plastic and elastic damaged strain components. The terms $\varepsilon_t^{ck}$ and $\varepsilon_{0t}^{el}$ shown in Figure 6 represent the crushing and elastic undamaged strain components and similarly, $\varepsilon_t^{pl}$ and $\varepsilon_t^{el}$ show plastic and elastic damaged strain components, respectively, in tensile region.

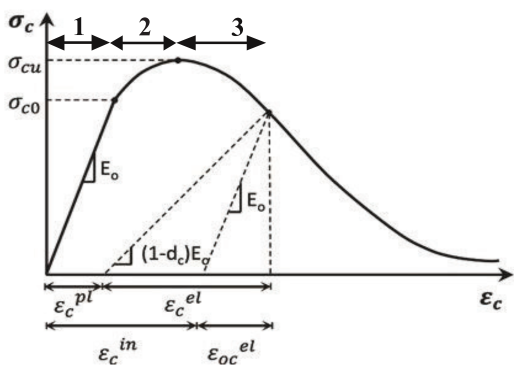


**Figure 5 - Compressive Stress Strain Curve for Concrete [23]**

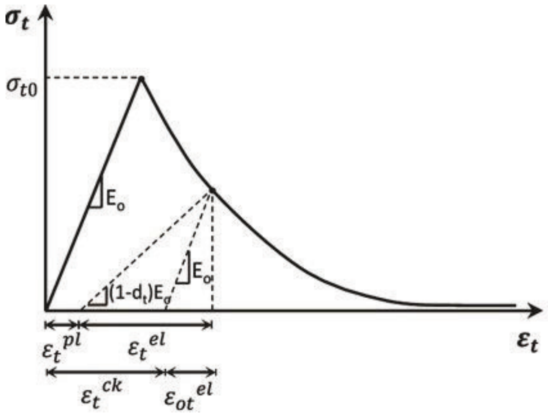


**Figure 6 - Tensile Stress Strain Curve for Concrete [23]**

As shown in Figure 5, the compressive behaviour of the concrete can be divided into three regions. The first region is linear and that can be represented by $\sigma_{c(1)} = E_0\varepsilon_c$, reaching up to $0.4\sigma_{cu}$. The behaviour in the second region from $0.4\sigma_{cu}$ to $\sigma_{cu}$ can be represented by Eq. (1).

$$\sigma_{c(2)} = \frac{E_{c_i}\frac{\varepsilon_c}{\sigma_{cu}} - \left(\frac{\varepsilon_c}{\varepsilon_{cm}}\right)^2}{1 + \left(E\frac{\varepsilon_{cm}}{\sigma_{cu}}\right)\frac{\varepsilon_c}{\varepsilon_{cm}}}\sigma_{cu} \qquad ...(1)$$

The third region of the curve is given by Eq. (2). In Eqs. (2) and (3), $G_{ch}$ is the crushing energy per unit area and $l_{eq}$ is the characteristic length. Experimental results were given with b=0.9 as an initial guess [22].

$$\sigma_{c(3)} = \left(\frac{2 + \gamma_C\sigma_{cu}\varepsilon_{cm}}{2f_{Cm}} - \gamma_c\varepsilon_c + \frac{\varepsilon_c^2\gamma_C}{2\varepsilon_{cm}}\right)^{-1} \qquad ...(2)$$

$$\gamma_C = \frac{\pi^2\sigma_{cu}\varepsilon_{cm}}{2\left[\frac{G_{ch}}{l_{eq}} - 0.5\sigma_{cu}\left(\varepsilon_{cm}(1-b) + b\frac{\sigma_{cu}}{E_0}\right)\right]^2};\ b = \frac{\varepsilon_c^{pl}}{\varepsilon_c^{ch}} \qquad ...(3)$$

Considering the tensile behaviour of the concrete, the ratio between tensile stress $\sigma_t(w)$ and maximum tensile strength $\sigma_{t0}$, is given in Eq. (4). In Eq. (4), $c_1 = 3$, $c_2 = 6.93$ [24], and $w_c$ is the critical crack opening.

$$\frac{\sigma_t(w)}{\sigma_{to}} = \left[1 + \left(c_1\frac{w}{w_c}\right)^3\right]e^{-c_2\frac{w}{w_c}} - \frac{w}{w_C}(1 + c_1^3)e^{-c_2} \qquad ...(4)$$

The above-mentioned model was used to define concrete material properties in this study. Defined parameters for the CDP model are shown in Table 1. Figures 7 and 8 show the developed stress-strain and damage models for compression and tension.

**Table 1 - Parameters for CDP Model**

| Parameter | Value |
|---|---|
| Dilation angle | 13 |
| Eccentricity | 0.1 |
| $F_{bo}/F_{co}$ | 1.16 |
| K factor | 0.666 |
| Viscosity | 0.0001 |

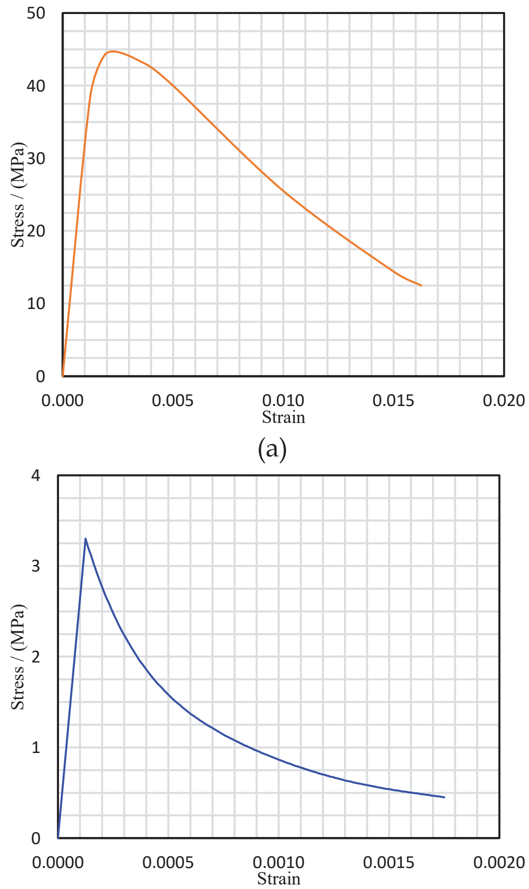


(a)

(b)

**Figure 7 - Stress-Strain Curves of Concrete: (a) Compressive Behaviour and (b) Tensile Behaviour**

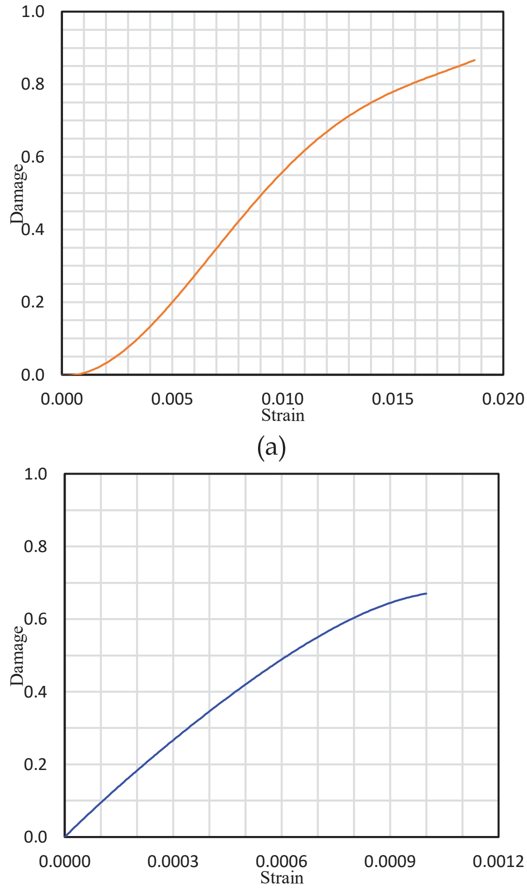


(a)

(b)

**Figure 8 - Damage-Strain Curves of Concrete: (a) Compressive Behaviour and (b) Tensile Behaviour**

### 2.1.2 Steel Material Properties

The steel material model has a huge impact on the accuracy of the numerical model. The yield criterion and the hardening model play a key role in the steel material model. The von mises yield criterion is used in most studies considering steel as an isotropic material. Hardening is the change of yield surface as material yields. There are three different hardening rules [25] called Isotropic Hardening, Kinematic Hardening and Combined Hardening. The combined hardening model is used for this study which captures the expanding and translation of the yield surface of the material in a realistic manner. Material properties for the SM490 material is shown in Table 2 and the elasto-plastic bilinear stress strain model for SM490 [26] which was used in the simulations as shown in the Figure 9. In addition, the combined hardening model was implemented with the von-mises yield criterion in ABAQUS to capture the inelastic behaviour of the material under cyclic hardening.

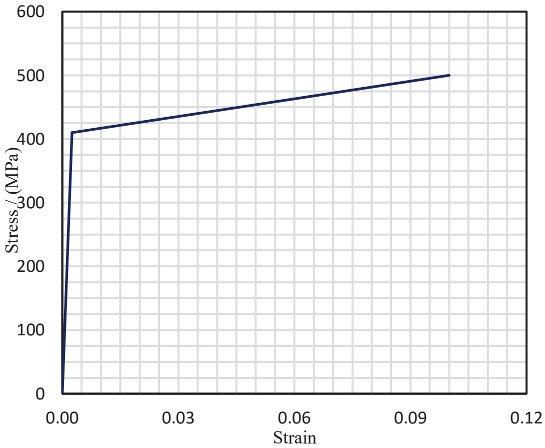


**Figure 9 – Bilinear Material Model used for the Simulation**

**Table 2 - Material Properties of Steel (SM490)**

| Parameter | Value |
|---|---|
| Yields stress ($\sigma_y$) | 308 MPa |
| Young's modulus ($E_s$) | 211000 MPa |
| Ultimate stress ($\sigma_u$) | 455 MPa |
| Poisons ratio (v) | 0.27 |

## 2.2 Numerical Modelling

FE model of the CFST column consists of a concrete core encased in steel plates and diaphragms. The steel column and the concrete core were modelled using C3D8R solid elements available in the *ABAQUS* software, which has three translational degrees of freedom in each 8 nodes. The interaction between concrete and steel was modelled using the surface-to-surface connection with the tangential friction coefficient of 0.4 and hard interaction between steel and concrete. Tie connections were used to connect diaphragms to the steel and concrete sections. Figure 10 shows the components of the FEM model for the CFST column. Diaphragms which are shown in Figure 10 are used to enhance the load bearing capacity of the column section.

All degrees of freedom of the steel and concrete are restrained at the base surface of the column to represent a fixed support at the base. Several models were analysed with different mesh arrangements to identify the optimum element size of the mesh for the analysis. The base shear was plotted against the number of elements in each analysis and the optimum size of the elements was identified as 15 mm using the mesh sensitivity analysis.

## 2.3 Loading

Initially, an axial load *P* was applied with the $P/P_y$ ratio of 0.125 ($P_y = A_s\sigma_y$, where $A_s$ is the cross-sectional area of the steel section and $\sigma_y$ is the yield strength). A three-cycle reversal cyclic loading pattern shown in Figure 11 was applied to simulate the earthquake behaviour. This type of cyclic loading pattern stabilizes the material behaviour at each strain level before increasing the strain levels. Such loading patterns are commonly used in experimental setups [1].

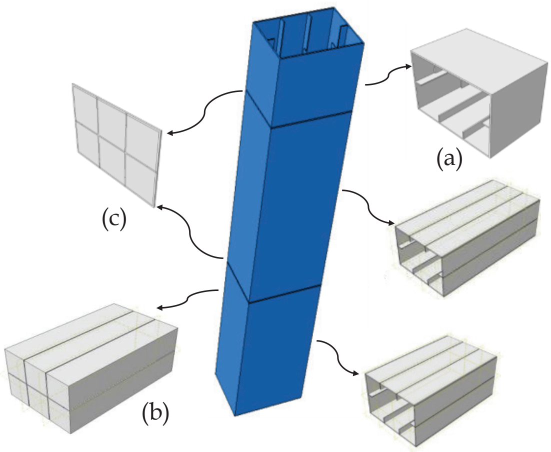


**Figure 10 - Components of the FEM Model: (a) Steel Sections (b) Concrete Core and (c) Diaphragms**

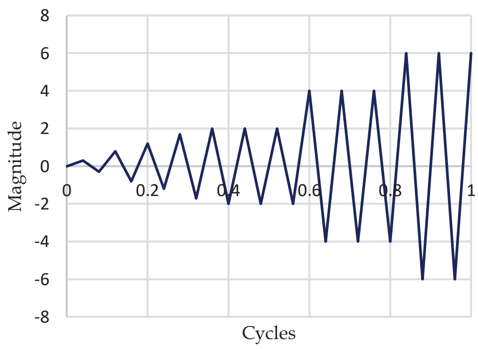


**Figure 11 - Cyclic Loading Pattern [1]**

## 2.4 Specimen Geometry

The first finite element model was developed with the exact dimensions of the previous experimental test specimen [24] for the validation purpose. Then, several models were developed altering the stiffener arrangements for the parametric study.

#### 2.4.1 Details of the Experimental CFST Columns (Validation)

Experimental study conducted on the CFST columns with stiffener by Usami et al. (1996) [1] was selected for the validation of the numerical model of CFST columns. Height of the steel column and the height of concrete column were 1854 mm and 668 mm, respectively. Further, the geometric parameters for the column section were, b=418 mm, D=264 mm, steel plate thickness=5.87 mm, stiffener thickness ($t_s$)=4.27 mm, stiffener length ($b_s$)=34 mm (see Figures 12 and 13).

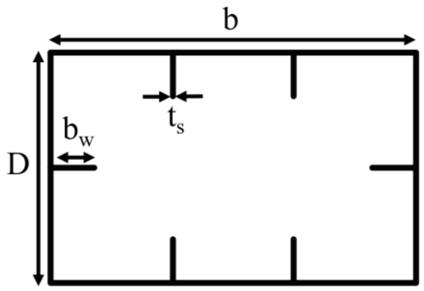


**Figure 12 - Dimensions of the Specimen Cross-Section**

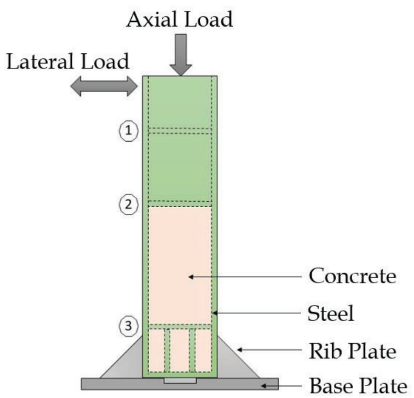


**Figure 13 - Sectional View of the Specimen**

#### 2.4.2 Parametric Study

In the next step, effect of each cross-sectional parameter on confinement (see Figure 14 and Table 3) was evaluated through a parametric study using validated FE model. The study was conducted to identify the section which gives the maximum confinement effect on concrete, hence improving the seismic performance. Study was carried out in three major steps. Frist, the $L_w/L_p$ ratio (stiffener length to spacing ratio, where $L_p$ is the spanning ratio of stiffeners in the longer direction) was varied in ratios of 0.20, 0.26, 0.34 by varying the stiffener length $L_w$, and the ratio which gives the maximum seismic performance was identified. Next, the same $L_w/L_p$ ratio identified in the previous step was applied for four sections with different stiffener arrangements shown in Figure 15 to select the stiffener arrangement which has the maximum seismic performance. Then, by altering the $L_f/L_w$ ratio initially by changing the $L_f$ while $L_w$ is fixed and next by keeping the $L_f$ fixed and changing $L_w$, best $L_f/L_w$ was identified for maximum strength and maximum ductility.

This parametric study investigates the effect of confinement in concrete towards the column strength, ductility and energy absorption capacity. Table 3 gives the summarization of the dimensions of each specimen.

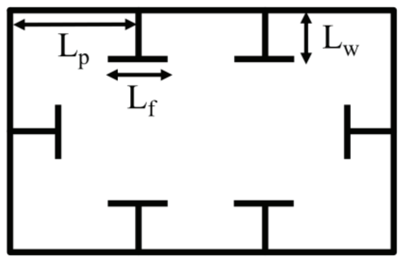


**Figure 14 - Cross Section of the CFST with Stiffeners**

**Table 3 - Parameters for the Parametric Study**

| Section | $L_f$(mm) | $L_w$(mm) | $L_p$(mm) | I (mm$^2$)x10$^6$ | h (mm) | $\sigma_y$ (MPa) | $H_y$ (kN) | $\delta_y$ (mm) |
|---|---|---|---|---|---|---|---|---|
| (a) Set $L_f$=0 and change the $L_w/L_p$ (stiffener length to spacing ratio) | | | | | | | | |
| $L_w$ / $L_p$ = 0.20 | 0 | 25 | 132 | 592.3 | 1680 | 38.2 | -31.5 | -3.3 |
| $L_w$ / $L_p$ = 0.26 | 0 | 34 | 132 | 590.7 | 1680 | 38.2 | -33.1 | -3.3 |
| $L_w$ / $L_p$ = 0.34 | 0 | 45 | 132 | 589.0 | 1680 | 38.2 | -31.3 | -3.3 |
| | | | | | | | | |
| (b) change the stiffener arrangement | | | | | | | | |
| Arrangement 1 | 0 | 34 | 132 | 590.7 | 1680 | 38.2 | -33.1 | -3.3 |
| Arrangement 2 | 0 | 34 | 87 | 586.8 | 1680 | 38.2 | -31.2 | -3.3 |
| Arrangement 3 | 0 | 34 | 87 | 585.6 | 1680 | 38.2 | -31.2 | -3.3 |
| Arrangement 4 | 34 | 34 | 132 | 585.4 | 1680 | 38.2 | -31.1 | -3.3 |
| | | | | | | | | |
| (c) change the flange to web ratio ($L_f/L_w$) | | | | | | | | |
| $L_f$ / $L_w$ = 0.80 | 34 | 44 | 132 | 584.8 | 1680 | 38.2 | -31.1 | -3.3 |
| $L_f$ / $L_w$ = 1.00 | 34 | 34 | 132 | 585.4 | 1680 | 38.2 | -31.1 | -3.3 |
| $L_f$ / $L_w$ = 1.40 | 34 | 25 | 132 | 585.9 | 1680 | 38.2 | -31.2 | -3.3 |
| $L_f$ / $L_w$ = 1.50 | 51 | 34 | 132 | 582.6 | 1680 | 38.2 | -31.0 | -3.3 |
| $L_f$ / $L_w$ = 2.00 | 68 | 34 | 132 | 605.6 | 1680 | 38.2 | -32.2 | -3.3 |

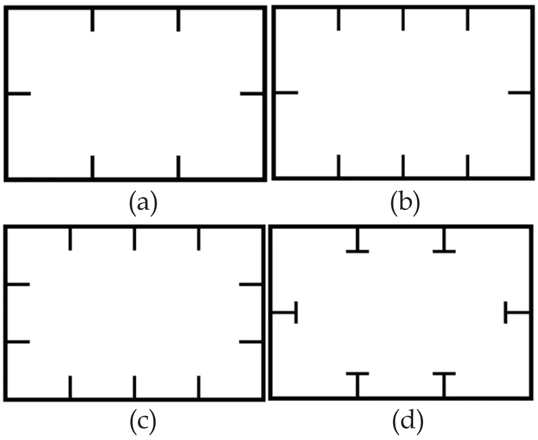


**Figure 15 - Stiffener arrangements: (a) Arrangement 1 (b) Arrangement 2 (c) Arrangement 3 and (d) Arrangement 4**

By exploring the variations of the results from initial step, adjustments were done to the spacing and geometry of the stiffeners. As a final step, modifications were done on the stiffener Arrangement 4 by comparing the maximum strength values obtained from the step two. Flange length ($L_f$) and web length ($L_w$) of the stiffeners were changed to obtain the different $L_f/L_w$ (flange to web length) ratios of 0.8, 1.4, 1.5 and 2.0. The steel column height=1854 mm, concrete height=668 mm, b=418 mm and D=264 mm parameters were kept same as the validated model. Finally. the section which gives the maximum confinement effect on concrete, resulting in improved lateral performance of the structure, was identified.

When comparing the results obtained for different cross-sections, to normalize the area effect and the shear effect of the different cross sections, the following equations from Yuan et. al., 2021 [28] which are presented in Eq. (5) and Eq. (6) were used where, $H_y$ denotes the lateral yield load and $\delta_y$ denotes corresponding lateral yield displacement.

$$\delta_y = \frac{H_0 h^3}{3EI} + \frac{H_0 h}{kGA} \quad \text{...(5)}$$

$$H_y = \left(\sigma_y - \frac{P}{A}\right)\frac{z}{h} \quad \text{...(6)}$$

where,
$H_y$ = Lateral yield load
$\delta_y$ = Lateral yield displacement
$\sigma_y$ = Yield strength of the steel
k = Transverse shear stiffness ratio (0.53)
G = Shear modulus
z = Section modulus
h = column height
P = Applied axial load
A = Cross sectional area of steel section

# 3. Results

## 3.1 Validation of the FEM Model

The lateral load displacement hysteresis curves from the numerical simulations were compared with the available resultant experimental curves in the literature. As shown in Figure 16, the numerical hysteresis curves show good agreement with the experimental curves. Minor deviations from the experimental curves may have occurred due to the material irregularities, residual stresses and initial imperfections in experimental setup. Due to the presence of the concrete core, the buckling has shifted away from the base of the column to the top of the concrete section as shown in Figure 17.

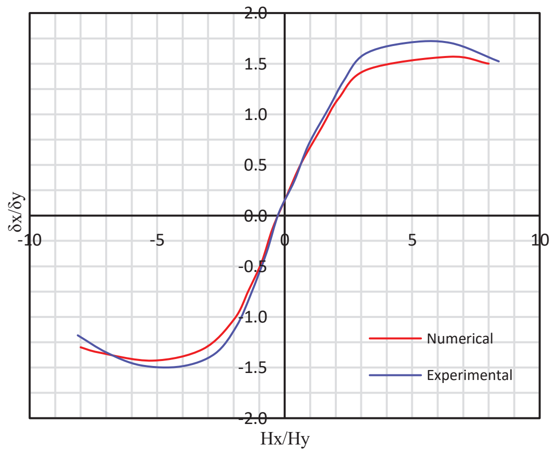


**Figure 16 - Comparison of the Experimental and Numerical Graphs for the CFST with Stiffeners**

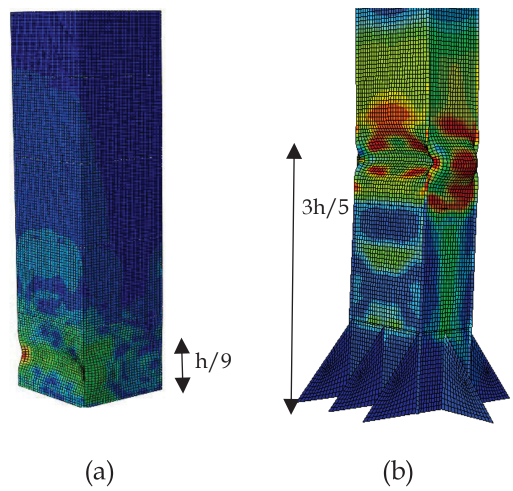


**Figure 17 - Comparison of the Buckling Heights in (a) Steel Column without Concrete and (b) CFST Column**

## 3.2 Effect of the Stiffener Length ($L_w$/ $L_p$) on Confinement

At the initial stage, stiffener length ($L_w$) is changed and $L_f$ was set to zero. In order to observe the effect of confinement in concrete in various section layouts, principal stresses of the section cuts at 200 mm, 400 mm and 600 mm from the bottom was compared for the 7th cycle. Figure 18 illustrates the plan view of each cross section at different levels from the bottom and the normalized envelope curves for each case are shown in Figure 19. According to Figure 18, the maximum principal stresses were obtained at 200 mm level. This result shows the maximum confinement was obtained near the base level of the column. After obtaining the maximum confinement at the bottom, confinement is reduced gradually towards the column top.

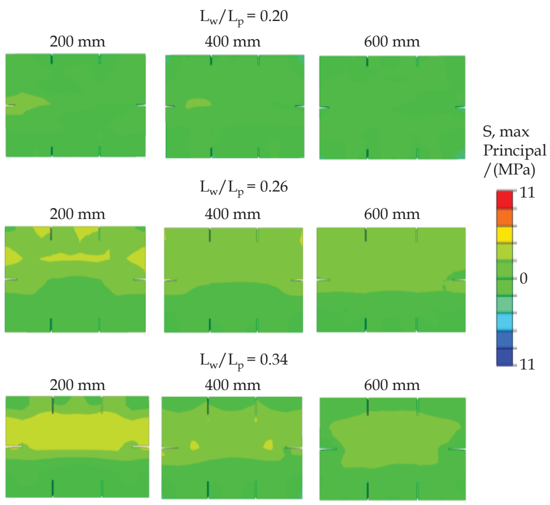


**Figure 18 - Principal Stresses Variation of Concrete Cross-Sections for the different $L_w/L_p$ Ratios**

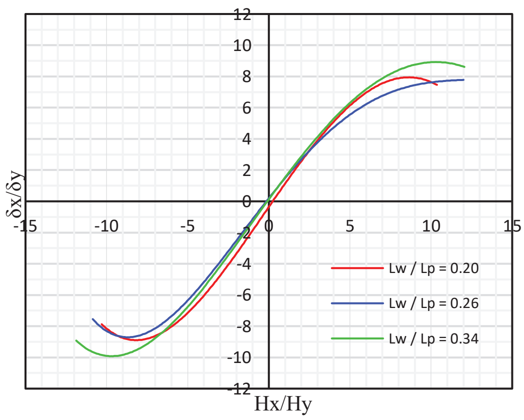


**Figure 19 - Normalized Envelop Curves for the different $L_w/L_p$ Ratios**

As shown in Table 4, the maximum strength ($H_m/H_o$) and the strength value corresponding to the 95% of the displacement ($H_{95}/H_o$) is calculated for further analysis.

**Table 4 - Strength Values for the different $L_w/L_p$ Ratios**

| $L_w/L_p$ | $H_m/H_o$ | $D_m/D_o$ | $H_{95}/H_o$ |
|---|---|---|---|
| 0.2 | 8.0 | 10.4 | 7.6 |
| 0.26 | 7.9 | 12.0 | 7.51 |
| 0.34 | 9.0 | 12.1 | 8.55 |

Calculated strength values do not change significantly with different ($L_w$ / $L_p$) ratios. Therefore, further studies were conducted to find a better arrangement that gives higher confinement effect by changing the cross-sectional arrangement and $L_f/L_w$ ratio.

### 3.3 Effect of the Stiffener Arrangement on Confinement

Four cross-sections with different stiffener arrangements which were used in the next step to identify the arrangement which gives the maximum performance are shown in Figure 15. The resultant principal stresses which were obtained from the numerical simulations were compared at the levels of 200 mm, 400 mm, and 600 mm from the bottom for all four stiffener arrangements as shown in Figure 20.

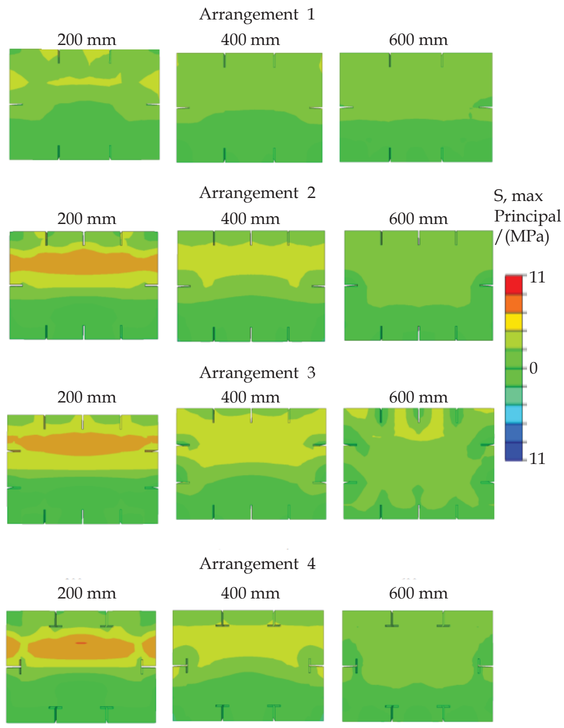


**Figure 20 - Principal Stresses Variation of Concrete Cross-Sections for different Cross-Sectional Arrangements**

Figure 21 shows the normalized envelop curves for each arrangement. From the results, it can be identified that Arrangement 4 has the maximum strength and ductility and the respective values are given in Table 5. Therefore, Arrangement 4 was chosen for further studies on the effect of confinement by changing the length ratios of the section.

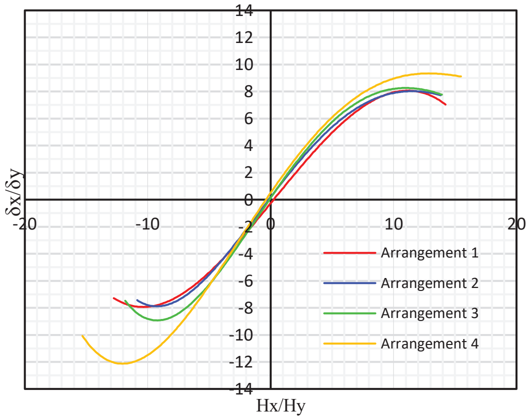


**Figure 21 – Normalized Envelop Curves for different Cross-Sectional Arrangements**

**Table 5 – Strength Values for different Cross-Sectional Arrangements**

| Arrangement | $H_m/H_o$ | $D_m/D_o$ | $H_{95}/H_o$ |
|---|---|---|---|
| 1 | 8.12 | 14.25 | 7.71 |
| 2 | 8.00 | 13.89 | 7.60 |
| 3 | 8.25 | 14.00 | 7.84 |
| 4 | 9.31 | 15.50 | 8.84 |

### 3.4 Effect of the ($L_f$/ $L_w$) Ratio on Confinement

Initially, the $L_f/L_w$ ratio was changed by varying the $L_f$ length in ratios of 1.0, 1.5 and 2.0 and obtained the principal stresses as shown in Figure 22.

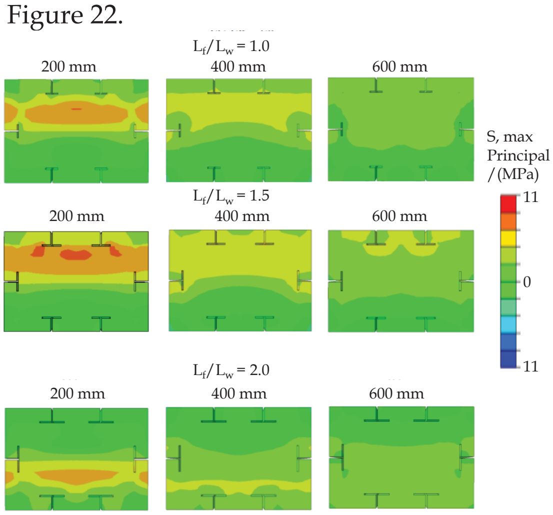


**Figure 22 – Principal Stresses Variation of Concrete Cross-Sections for the different $L_f$ / $L_w$ Ratios. (varying the $L_f$ length)**

Next, $L_f/L_w$ ratio was set to 0.8, 1.0 and 1.4 by varying the $L_w$ length and obtained the principal stresses as shown in Figure 23. Figure 24 shows all the normalized envelop curves corresponding to different $L_f/L_w$ ratios and the corresponding strength values are presented in Table 6.

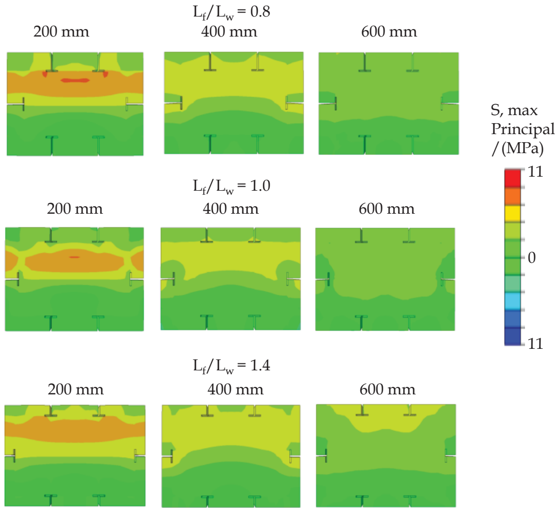


**Figure 23 – Principal Stresses Variation of Concrete Cross-Sections for the different $L_f$ / $L_w$ Ratios (vary the $L_w$ length)**

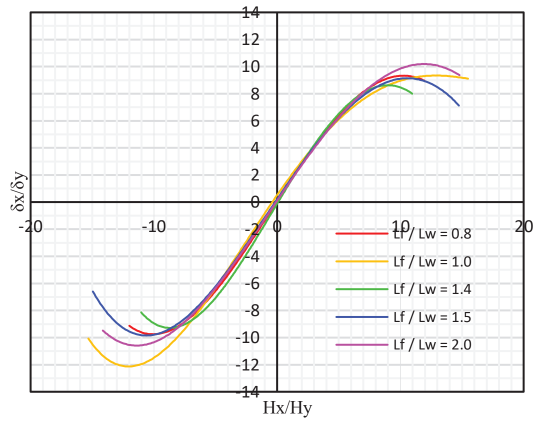


**Figure 24 – Normalized Envelop Curves for the different $L_f$/ $L_w$ Ratios.**

**Table 6 – Strength Values for the different $L_f$/ $L_w$ Ratios**

| $L_f/L_w$ | $H_m/H_o$ | $D_m/D_o$ | $H_{95}/H_o$ |
|---|---|---|---|
| 0.8 | 9.43 | 11.90 | 8.93 |
| 1.0 | 9.45 | 15.50 | 8.93 |
| 1.4 | 8.62 | 10.90 | 8.17 |
| 1.5 | 9.23 | 14.75 | 8.74 |
| 2.0 | 10.21 | 14.75 | 9.69 |

The performance values yield that the maximum strength achieved at $L_f/L_w$ = 2.0 while the maximum ductility is shown in $L_f/L_w$ = 1.0.

According to the results obtained by numerical simulations, the concrete confinement has enhanced in each step of the parametric study. It can also be observed that the strength, ductility and energy absorption capacity also increased with respect to the gradual increase of concrete confinement.

## 4. Conclusions

In this research, a numerical model was created and validated, and then a parametric study was carried out having four different stiffener arrangements and varying the length of the stiffeners to observe the effect of such parameters towards the confinement of concrete and the overall seismic performance of the CFST columns. From this study, it can be concluded that,

- The maximum principal stress exhibits a gradual increase with the rising $L_w/L_p$ ratio. Notably, the $L_w/L_p$ ratio of 0.2 demonstrates an early enhancement in maximum strength. However, it is important to note that this ratio comes with a trade-off, as the ductility is lower in comparison to the $L_w/L_p$=0.34 and 0.26. However, altering the $L_w/L_p$ ratio does not result in a substantial improvement in confinement.
- Stiffener Arrangement 4 exhibits the highest $H_m/H_o$ (lateral strength to yield lateral strength ratio), maximum ductility, due to the large confinement effect spread over the stiffeners.
- Further, modifying the $L_f/L_w$ ratio in Arrangement 4 results in additional improvements in confinement in the concrete. Specifically, $L_f/L_w$=2.0 yields the highest $H/H_y$ and maximum energy absorption capacity, whereas $L_f/L_w$=1.0 achieves the maximum ductility.
- $L_f/L_w$=2.0 gives the best cross-sectional arrangement for the strength and for the energy absorption capacity while $L_f/L_w$=1.0 is the best arrangement for the ductility criteria. However, when considering the overall performance in strength, ductility and energy absorption capacity, the cross-section with the ratio of $L_f/L_w$=2.0 can be identified as the best section.

The major failure mode identified in CFST piers under cyclic loading is the local buckling of side plates and stiffeners above the concrete filled section. By introducing proper techniques to strengthen the corners of the piers could enhance the overall performance in strength and ductility by delaying local buckling. Further research should be carried out on CFST bridge piers to understand the possibility of other failure modes such as initiation and propagation of brittle fracture due to accumulated low cycle fatigue under seismic loads and to discover possible strengthening methods to improve overall performance.


## Acknowledgement

The authors would like to acknowledge licensed applications of the ABAQUS package facilitated by the Finite Element Analysis and Simulation Centre, Rubber Research Institute of Sri Lanka, Ratmalana.


## References


1. Ge, H., Usami, T., "Cyclic Tests of Concrete-Filled Steel Box Columns", *Journal of Structural Engineering,* 1996, pp. 1169-1177

2. Zarringol, M., Thai, H.T., Thai, S. and Patel, V., "Application of ANN to the Design of CFST Columns", In *Structures* Elsevier, 28, 2020, December. pp. 2203-2220.

3. Thai, H.T., Thai, S., Ngo, T., Uy, B., Kang, W.H. and Hicks, S.J., "Reliability Considerations of Modern Design Codes for CFST Columns", Journal *of Constructional Steel Research*, 2021, *177*, p.106482.

4. Watanabe, E., K. Sugiura, K. Nagata, K. and Kitane., "Performances and Damages to Steel Structures during the 1995 Hyogoken-Nanbu Earthquake", *Engineering Structures* 20, No. 4-6 (1998). 282-290.

5. Zhou, D. and Li, R., "Damage Assessment of Bridge Piers Subjected to Vehicle Collision", *Advances in Structural Engineering*, *21*(15), 2018, pp.2270-2281.

6. Itoh, Y., Wada, M. and Liu, C., "Lifecycle Environmental Impact and Cost Analyses of Steel Bridge Piers with Seismic Risk", In *Proceedings of the 9th International Conference on Structural Safety and Reliability* (Vol. 273), 2005, June.

7. Kitada, T., "Ultimate Strength and Ductility of State-of-the-Art Concrete-Filled Steel Bridge Piers in Japan", *Engineering Structures*, *20*(4-6), 1998, pp.347-354.

8. Wang, Y., Yang, Y. and Zhang, S., "Static Behaviors of Reinforcement-Stiffened Square Concrete-Filled Steel Tubular Columns", *Thin-Walled Structures*, *58*, 2012, pp.18-31.

9. Yan-yan, Z.H.A.N., Lin, Z., Yu-wen, L.I.A.N.G., Jin-xin, C.A.O. and Yao-jun, G.E., "Comprehensive Assessment of Wind-Induced Interference Criteria about Large Cooling Towers with Typical Six-Towers Double-Columns Arrangements", 2017, 工程力学, *34*(11), pp.66-76.

10. Guo, L., Zhang, S., Kim, W.J. and Ranzi, G., "Behavior of Square Hollow Steel Tubes and Steel Tubes Filled with Concrete", *Thin-Walled Structures*, *45*(12), 2007, pp.961-973.

11. Han, X., Jiang, A., Zheng, J., Zhou, X., Chen, Y., Fang, S., Li, X., He, J. and Li, H., "Seismic Behavior of Box Steel Bridge Pier with Built-In Energy Dissipation Steel Plates", *Advances in Materials Science and Engineering*, *2022*.

12. Wang, Z.B., Han, L.H., Li, W. and Tao, Z., "Seismic Performance of Concrete-Encased CFST Piers: Experimental Study". *Journal of Bridge Engineering*, 2016, *21*(4), p.04015072.

13. Ge, H. and Usami, T.,"Cyclic Tests of Concrete-Filled Steel Box Columns", *Journal of Structural Engineering*, *122*(10), 1996, pp.1169-1177.

14. Thevega, T., Rajavijayan, K., Jayasinghe, J.A.S.C. and Susantha, K.A.S. "Strength and Ductility of Stiffened Steel Box Columns of Various Cross-Sectional Configurations under Lateral Cyclic Loadings", *Journal of Institution of Engineers, 2021,* pp. 25-32.

15. Dong, C. and Ho, J.C.M., "Improving Interface Bonding of Double-Skinned CFST Columns" *Magazine of Concrete Research*, 2013, *65*(20), pp.1199-1211.

16. Raza, A., ur Rehman, A., Masood, B. and Hussain, I., "Finite Element Modelling and Theoretical Predictions of FRP-Reinforced Concrete Columns Confined with Various FRP-Tubes", In *Structures* (Vol. 26, 2020, August, pp. 626-638). Elsevier.

17. Dabaon, M., El-Khoriby, S., El-Boghdadi, M. and Hassanein, M.F., "Confinement Effect of Stiffened and Unstiffened Concrete-Filled Stainless Steel Tubular Stub Columns" *Journal of Constructional Steel Research*, 2009, *65*(8-9), pp.1846-1854.

18. Jenothan, M., Jayasinghe, J.A.S.C., Bandara, C.S., "Lateral Behaviour and Performance Evaluation of Steel Piers under Cyclic Lateral Loading", *J. Constr. Steel Res. 201 (2023)* 107764.

19. Gao, S., Usami, T. and Ge, H., "Ductility Evaluation of Steel Bridge Piers with Pipe Sections", *Journal of Engineering Mechanics*, 1998, pp. 260-267.

20. Cocchetti, G. and Maier, G., "Elastic–Plastic and Limit-State Analyses of Frames with Softening Plastic-Hinge Models by Mathematical Programming", *International Journal of Solids and Structures*, *40*(25), 2003, pp.7219-7244.

21. Bayrak, O. and Sheikh, S.A., "Plastic Hinge Analysis", *Journal of Structural Engineering*, *127*(9), 2001, pp.1092-1100.

22. B. Alfarah, F. López-Almansa, S. Oller, New Methodology for Calculating Damage variables evolution in plastic damage model for RC structures, *Eng. Struct.* 132 (2017) 70-86,

23. ABAQUS, Abaqus 6.14, Abaqus 6.14 Anal. User's Guide. (2014) 14.

24. CEB-FIP, CEBFIP, Model code 2010, EuroInternational Du Bet. 594 (2010).

25. Usami, T. and Ge, B.H., "Cyclic Behavior of Thin-Walled Steel Structures- numerical analysis", *Thin-Walled Structures* 32, 1998.

26. Susantha, K. A. S., Aoki, T. and Jayasinghe, R.T.M., "Finite Element Analysis of Steel Columns Subjected to Bi-Directional Cyclic Loads", *Journal of Institution of Engineers*, 2007, pp. 35-41.

27. Chen, X., Bu, J. and Xu, L., "Effect of Strain Rate on Post-Peak Cyclic Behavior of Concrete in Direct Tension" *Construction and Building Materials*, 2016, 124, pp.746-754.

28. Yuan, H.H., Dang, J., Wu, Q.X. and Aoki, T., "A Modified Curve-Approximated Hysteretic Model for Partially Concrete-Filled Steel Tube Bridge Piers", *Journal of Constructional Steel Research*, 2021, *185*, p.106861.